water

MDPI

Article

Constraining the Water Cycle Model of an Important Karstic Catchment in Southeast Tibetan Plateau Using Isotopic Tracers (^{2}H, ^{18}O, ^{3}H, ^{222}Rn)

Dawei Liao [1,2,3], Zhonghe Pang [1,2,3,*], Weiyang Xiao [4], Yinlei Hao [1,2,3], Jie Du [4], Xiaobo Yang [5] and Geng Sun [6]

1 Key Laboratory of Shale Gas and Geoengineering, Institute of Geology and Geophysics, Chinese Academy of Sciences, Beijing 100029, China; david.liao@mail.iggcas.ac.cn (D.L.); ylhao@mail.iggcas.ac.cn (Y.H.)
2 Innovation Academy for Earth Science, Chinese Academy of Sciences, Beijing 100029, China
3 College of Earth and Planetary Sciences, University of Chinese Academy of Sciences, Beijing 100049, China
4 Jiuzhaigou Nature Reserve Administrative Bureau, Zhangzha Town, Jiuzhaigou 623402, China; x15279632663@126.com (W.X.); l15683837124@163.com (J.D.)
5 Aba Bureau of Hydrology and Water Resources Survey, Wenchuan 623000, China; JZGXWY@163.com
6 China-Croatia "Belt and Road" Joint Laboratory on Biodiversity and Ecosystem Services, Chengdu Institute of Biology, Chinese Academy of Sciences, Chengdu 610041, China; sungeng@cib.ac.cn
* Correspondence: z.pang@mail.iggcas.ac.cn; Tel.: +86-10-8299-8613

Received: 6 October 2020; Accepted: 17 November 2020; Published: 24 November 2020

check for updates

Abstract: Understanding the connectivity between surface water and groundwater is key to sound geo-hazard prevention and mitigation in a waterscape such as the Jiuzhaigou Natural World Heritage Site in the southeast Tibetan Plateau, China. In this study, we used environmental isotope tracers (^{2}H, ^{18}O ^{3}H, and ^{222}Rn) to constrain a water cycle model including confirming hydrological pathways, connectivity, and water source identification in the Jiuzhaigou catchments. We established the local meteoric water line (LMWL) based on the weekly precipitation isotope sampling of a precipitation station. We systematically collected water samples from various water bodies in the study area to design the local water cycle model. The regional water level and discharge changes at one month after the earthquake indicated that there was a hydraulic connection underground across the local water divide between the Rize (RZ) river in the west and Zechawa (ZCW) lake in the east by the $\delta^{18}O$ and $\delta^{2}H$ measurements. We employed an end-member mixing model to identify and quantify Jiuzhaigou runoff-generating sources and their contributions, and we found that the average contributions of precipitation and groundwater to the surface runoff in the catchments are about 30% and 70%, respectively. The two branches of the Shuzheng (SZ) trunk were recharged by 62 ± 19% from the ZCW lake and 38 ± 19% from the RZ river, which was consistent with the fractions calculated by the actual discharge volume. ^{222}Rn mass balance analyses were employed to estimate the water exchange between groundwater and river, which further confirmed this estimate. ^{222}Rn concentrations and ^{3}H contents showed that the groundwater had a short residence time and it was moderate precipitation, thought the contribution of groundwater to the river was 70%, according to the different tracers. A three-dimensional conceptual model of the water cycle that integrated the regional hydrological and geological conditions was established for the catchments.

Keywords: hydraulic connection; end-member mixing model; ^{222}Rn; groundwater–surface water interactions; Jiuzhaigou; Changhai Lake; water cycle model

1. Introduction

Investigations of connectivity between surface water and groundwater are pretty common because such connectivity plays an important role in maintaining water resources and the ecosystem of river basins [1–5]. Therefore, a complete understanding of the water exchange direction and water flux between groundwater and surface water is good to determine water balance and groundwater discharge in the protection of the natural flow regime of rivers [6]. Investigations of the evaluation, transformation, and connectivity of two sources play critical roles in their hydrological and ecological functions. A variety of methods of investigation between surface water and groundwater interactions include hydraulic tests [7], groundwater numerical models [3], environmental tracer methods [8–14], groundwater residence time and dating methods [15–17], and natural heat tracing methods [16,18,19]. Water bidirectional exchange can be effectively determined and quantified by environmental tracers, such as the stable water isotopes (^{2}H and ^{18}O), ^{222}Rn, and ^{3}H, as well as water chemical composition.

^{2}H and ^{18}O isotopes are useful and mature tracers in tracing the natural water cycle and different hydrological processes, such as hydrological pathways, water connectivity, water source identification, water evaporation, water mixing, and water exchange [20]. By combining geological conceptual models with isotope data, the hydraulic connection of aquifers or groundwater and surface water has been demonstrated in several studies [21–24]. The Milk River Aquifer–Aquitard systems of Canada were used as a model to test aquifer hydraulic connection with ^{2}H, ^{18}O, and chemical composition, and it was shown that it was difficult for surface water to mix downward with deep groundwater due to upper impermeable layers [22]. In the Xi'an area of China, the hydraulic connection between the upper Quaternary aquifer and the lower Tertiary aquifer was confirmed based on the ^{2}H, ^{18}O, ^{3}H, and ^{14}C tracing method [24]. In the Presciano Spring System of the Gran Sasso Carbonate Aquifer of Italy, homogeneous water isotope composition was found to indicate the existence of a buried karst conduit and baseflow pathway after the 2009 L'Aquila earthquake [23]. In northeastern Kansas, USA, potential hydraulic connections of local lowland aquifers with the surface water of a nearby creek and two major rivers were proven to exist based on identical ^{2}H and ^{18}O isotopes [21].

A major earthquake (Mw = 6.5 of mainshock) struck the Natural World Heritage Site Jiuzhaigou national park on August 8, 2017. Plenty of geologic hazards and damages were caused in the Rize (RZ) river and Shuzheng (SZ) valley. These disasters included debris flow, landslides, collapses, dam breaks of lakes, severely damaged roads, and destroyed surface landscapes [25,26]. The waterscape was especially damaged, with the Sparking Lake gone due to dam break, Nuorilang Waterfall being cut off (accompanied by cracking and shedding), and the section of the west valley having gathered water during our sampling period (Figure 1). There have been few investigations into the water connectivity and interaction between groundwater and surface water as an important karstic catchment of Jiuzhaigou in the southeast Tibetan Plateau, especially after the Jiuzhaigou earthquake. Based on observations of the regional water level at one month after the earthquake, the lake water level of the Zechawa (ZCW) valley in the east decreased. However, the stream discharge of the RZ river in the west was found to have been increasing. The Jiuzhaigou water cycle system seemed sensitive to earthquake activities. Thus, the post-earthquake investigation of the regional hydraulic connection between the eastern and western valleys was of significance to understand the groundwater circulation process under the earthquake pulse. The water exchange between groundwater and surface water and water source identification are vital for the karst water resource management and geo-hazard prevention of waterscapes in Jiuzhaigou.

The purpose of this research was to identify regional water connectivity, investigate interactions between surface water and groundwater, and establish a groundwater circulation model in the Jiuzhaigou catchments. We carried out an isotopic geochemical and hydrochemical measurements combining the regional surface water level and streamflow changes caused by the earthquake to (1) establish the local meteoric waterline and identify the flow path with ^{2}H and ^{18}O, (2) quantify Jiuzhaigou river water-generating sources and their contributions with different tracing methods,

(3) estimate the water exchange between groundwater and river with ^{222}Rn, and (4) develop a conceptual three-dimensional water cycle model by integrating regional hydrological and geological conditions.

Figure 1. Several waterscapes affected by the Jiuzhaigou earthquake: (**a**–**d**) represent the Nuorilang Waterfall cutoff, the dried-up Sparking Lake, a section of road in the west valley filled with water, and the Sparking Lake dam break, respectively.

2. Study Area

Jiuzhaigou, located in a northern region of Sichuan Province, China (Figure 2), has been designated as a World Heritage Site by UNESCO (United Nations Educational, Scientific, and Cultural Organization) since 1992. It is known for karst lakes and waterfalls, shoals, streams, travertines, snow peaks, and colorful forests [27]. It is composed of three main valleys in a "Y" shaped intersection of the western RZ valley, eastern ZCW valley, and middle SZ valley, as shown in Figure 2b. There is a watershed boundary with a 4200-m mountain ridge that controls the distribution of surface flow in the RZ and ZCW valleys, as seen in Figure 2c. The RZ valley in the west is always filled with surface water, linking a series of bead-distributed high mountain lakes, whereas the ZCW valley in the east has a perennial drought, with four separate lakes. As one of the most representative lakes in ZCW, Changhai Lake is 4350 m long, 250 m wide, 80 m deep, and the largest and highest glacier-dammed lake without a visible outlet. It has a total storage capacity of 45 million m^3. It is considered an important natural reservoir for water supply resources and regulation in the park, and it is located at 3075 m asl [28,29]. The Jiuzhaigou area is typical of a high plateau temperate and sub-Cambrian monsoon climate. The average annual precipitation is 880 mm, and the average annual temperature is 7.2 °C according to ZCW meteorological station (located at 2400 m asl) records. Precipitation mainly falls in the high-water season from May to October.

The strata in the Jiuzhaigou region from old to new are comprised of Devonian limestone and sandstone, Carboniferous limestone and slate, Permian limestone, Triassic limestone with dolomite, and Quaternary travertines with alluvial and glacial deposits (see Figure 2a) [30]. A set of marine carbonate rocks was developed with an exposed area of 500 km^2 and a total thickness of about 4 km. The underground karstic fractured aquifers are the Devonian Yiwaigou Group formation with a thickness of 300 m and Carboniferous Minhe Group formation with a thickness of 1000 m, both deposited in the shallow and coastal marine sedimentary environment. The lower Devonian Dangduo group formation is composed of metamorphic quartzite sandstones with low porosity and is the impermeable stratum of the basement. Quaternary sediments are distributed along the riparian zones in the valleys with 20–30 m travertine deposits.

The Mw6.5 Jiuzhaigou earthquake occurred on 8 August 2017 and was located within the eastern margin of the Tibetan Plateau. Tectonically, it was the transition zone of two geomorphologic units that fall steeply from the Tibetan Plateau to the Sichuan Basin. The epicenter was located in the Jiuzhaigou catchments shown in Figure 2a. The earthquake ruptured along a hidden extension of the northern Huya Fault [31–34]. Based on the high precision relocated mainshock and aftershock sequence of the Jiuzhaigou earthquake, Fang et al. (2018) showed that the causative fault manifested SE-trending, with a sinistral strike-slip motion striking of 150°, a dip of 84°, a length of 42 km, and a depth of at least 20 km [31]. The seismogenic fault (F1) was inferred along the Jiuzhaigou Paradise-epicenter (Flowers Lake), and F2 was a secondary co-seismic fault according to a field geological survey, landslide distributions, and remote sensing interpretation (as shown in Figure 2a) [35,36]. The earthquake, as one of the most important geological tectonic activities, not only affected the fault structure at a regional scale but also the groundwater flow at an aquifer scale.

The active tectonic movement shaped the topography of Jiuzhaigou. It caused the destruction of carbonate rock strata, the formation of fractures, and the reactivation of faults, all of which played a controlling role in the underground runoff. The fractures that controlled the water system of the Jiuzhaigou area were mainly north-west thrust faults (Yingzhaodong Fault F3, Changhai Lake–Hanging Spring Fault F4, Heye Fault F7, and Zharu Fault F8) and north–south thrust faults (Jiuzhaigou Fault F5 and Zechawa Fault F6), as shown in in Figure 2a [26,30]. Plenty of NW–SE oriented folds and faults provided potential flow pathways into the neighboring ditches [29]. The F3 fault zone stretched into the Colorful Pond and Changhai Lake from Yingzhaodong in the western valley across the mountain. Its strike was 225°, and its dip angle was between 50° and 72°. It was a compression–torsion fault with a length of 18 km that cut the Carboniferous Minhe Group formation. Some localized fractured rocks in the high-permeability fault zones were found, and some sections were crushed and fractured. It intersected with the RZ valley, causing the outcrops of the RZ spring groups (S3, S4, and S5) with a steady discharge volume of 1.74 m^3/s in the high-water season and 1.38 m^3/s in the low-water season [30]. F4 with an attitude of NE47° ∠67–72° and a length of 15 km was also a shattered cross-mountain fracture zone. It was characterized by fragmented rocks and well-developed fissures. Its south-eastern end extended into Changhai Lake of the eastern valley, and the north-western end was the Hanging Spring of the western valley. The Hanging Spring (S2) was located at the RZ valley and F4 fault intersection, the discharge of which was 0.29 m^3/s. F3 and F4 acted as good conductors for karst underflow and groundwater transport [28]. Along with S–N orientation, the F5 fault had a length of 25 km and an attitude of 100° ∠70–75°. It stretched along the RZ river and cut the carbonate aquifer. The F6 fault with an attitude of 280° ∠70–78° and a length of 20 km originated from Changhai Lake via the lower seasonal lake, and it stretched toward the eastern slopes of the Reed Lake in the SZ valley. F5 and F6 were both tensile–shear stretching faults that were good conductors to control groundwater flow from south to north. The Jiuzhaigou lakes and rivers were mainly distributed along F5 and F6. Most discharges flowed into karst lakes and rivers via many springs along the RZ and SZ rivers. As the source of the RZ river upstream in the Primeval forest, the S1 spring fed into the RZ river with a discharge volume of 6.81 m^3/s in the high-water season and 2.41 m^3/s in the low-water season. The discharge of the SZ spring groups (S8 and S9) was only 51–66 L/s in the SZ river. The annual average discharge of these springs was 6.33 m^3/s, accounting for about 49% of the surface runoff discharge [30]. They were important natural resources to maintain the waterscapes in the Jiuzhaigou catchments.

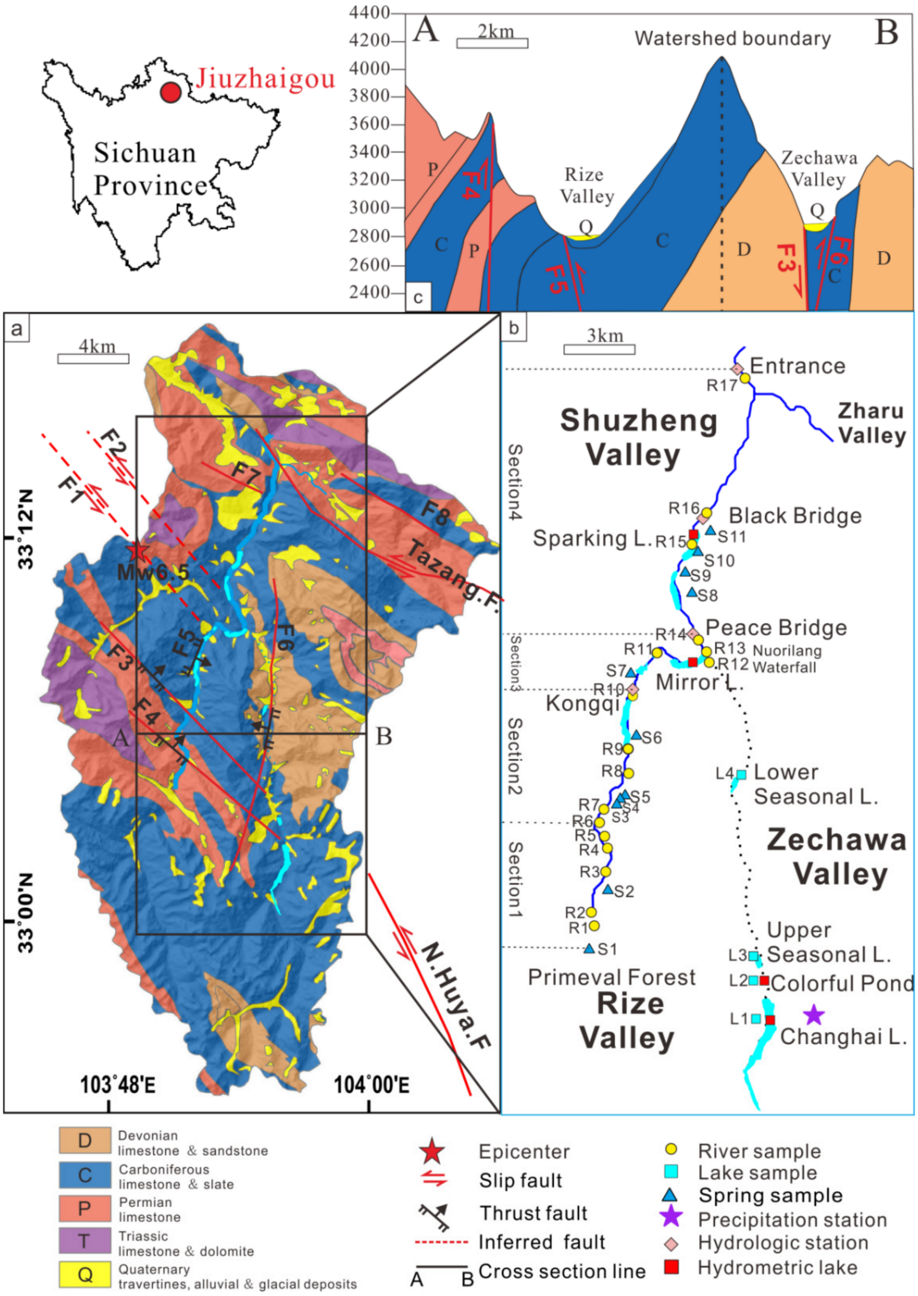

Figure 2. (**a**) Sketch map of Jiuzhaigou geological structure modified from the work of Lugli, 2017 [37]: (**b**) sampling sites in the (**c**) Jiuzhaigou section map. F1 is a seismogenic fault, and F2 is a secondary coseismic fault in the core predicted by Li and Wang [26,36]. F3–F8 are foregone thrust faults, referred to as the Yingzhaodong Fault (F3), the Changhai Lake–Hanging Spring Fault (F4), the Jiuzhaigou Fault (F5), the Zechawa Fault (F6), the Heye Fault (F7), and the Zharu Fault (F8), respectively.

3. Materials and Methods

A total of 32 water samples were collected during October 2019 along three valleys, which included surface water (river and lake water) and natural springs. Thirty-one weekly precipitation or snow samples were collected from October 2019 to June 2020 at the Changhai Lake precipitation station. Hydrological data (i.e., rainfall, stream discharge, and surface water level) were recorded and provided in the designated experimental ecological stations (four hydrologic stations and four hydrometric lakes) in the Jiuzhaigou catchments from January 2017 to December 2017 (one year in total before and after the earthquake) by Aba Prefecture Hydrographic Service in Sichuan. All sampling locations are presented in Figure 2b. We measured the water chemistry and isotopes of different water samples including the major ions, $\delta^{18}O$, δ^2H, ^3H, and ^{222}Rn. Based on the two-component isotope (^{18}O) hydrograph separation, we estimated the fractions of two tributaries (RZ and ZCW) in the mainstream (SZ) by combining the actual discharge volume. Additionally, the fractional uncertainty was quantified with the Gaussian error propagation technique. Based on the three-component isotope (^{18}O and total dissolved solid TDS) hydrograph separation, we calculated the fractions of local precipitation, Changhai Lake, and groundwater in Jiuzhaigou river water. We also employed the ^{222}Rn mass balance method to estimate the specific exchange between groundwater and river water and to calculate the groundwater proportion in river discharge.

3.1. Water Sampling and Analysis Method

Due to almost no wells or deep boreholes in the study area, 11 groundwater samples were collected from natural springs along the RZ and SZ rivers. We used different capacities of polyethylene bottles to directly collect the spring water from spring vents in order to avoid exchange with the atmosphere. The sites of S1–S7 springs were distributed mostly at the valley–fault intersections in the RZ valley. An intense-smelling H_2S appeared during the sampling of S3, S4, and S5 after the earthquake. The sites of the S8–S11 springs were distributed along the RZ valley, and 17 river water samples were collected along the RZ and SZ rivers from the Primeval forest to the entrance. Four sites of lake water were distributed along the ZCW valley in Changhai Lake, Colorful Pond, and the upper and lower seasonal lakes. We collected 31 weekly precipitation or snow samples at the Changhai Lake precipitation station. Prior to sampling, the water was filtered with the 0.45 μm membrane filters and stored in the high-density polyethylene bottles for measuring $\delta^{18}O$ and δ^2H, cations, anions, and tritium. A water sample of 250 mL at a depth of 10–15 cm under the surface of the water was collected in the vacuum bottles to measure the ^{222}Rn activity. The parameters measured and recorded in situ by using a portable multi-parameter controller (HQ40D, Hach) included pH and temperature. Before sampling, we calibrated the portable pH probes. A parameter-specific setting for pH probes, buffers set as the default modes (4.01, 7.01, and 10.01 as default), and a standard temperature value at 25 °C were firstly selected. Then, three standard solutions (pH = 4, 7, and 10) was prepared for pH calibration. The meter measured three values of the calibration solutions in order. If applicable, we chose to save the calibration. Alkalinity was titrated by a portable digital titrator (Digital Titrator 16900, Hach) in the field. The major ion analyses were determined by ion chromatography (Dionex ICS1100) (detection limit is 0.05 mg/L) in the Laboratory of Water Isotope and Water–Rock Interaction at the Institute of Geology and Geophysics, Chinese Academy of Sciences (IGG-CAS). The tritium contents were performed by electrolytic enrichment with a tritium enrichment factor of ~20 and the liquid scintillation counting (Quantulus 1220) method at the Analytical Laboratory of Beijing Research Institute of Uranium Geology. The tritium analytical precision was 0.4 TU. The $\delta^{18}O$ and δ^2H of all samples were measured by a Liquid Water Isotope Analyzer (Picarro L2130-i) in the Key Laboratory of Tibetan Environmental Changes and Land Surface Processes Chinese Academy of Sciences. The detection precisions were ±0.1‰ and ±0.4‰ for $\delta^{18}O$ and δ^2H, respectively. The ^{222}Rn content analysis was performed in the Key Laboratory of Groundwater Resources and Environment of Jilin University by the RAD-7 portable radon instrumentation (Durridge, Billerica, MA, USA) via radioactive decay accounts after sampling within two days. The measuring error was about 41% for groundwater and about 44% for surface water with all concentrations of ^{222}Rn.

3.2. End-Member Mixing Model

Two and three-component isotope hydrograph separation has been a powerful tool to calculate the ratio of various recharging sources in hydrologic studies [38–40]. It is based on the mass balance equations of water and tracer fluxes in a catchment [41]. The isotopic bivariate mixture model was used to estimate contribution in the mainstream (SZ) from tributaries (RZ and ZCW):

$$Q = Q_1 + Q_2 \quad (1)$$

$$Q\delta = Q_1\delta_1 + Q_2\delta_2 \quad (2)$$

where Q is the discharge and δ is the concentration of tracer. Subscripts 1 and 2 refer to ZCW and RZ tributaries, respectively.

As a fraction of local precipitation, Changhai Lake versus groundwater in Jiuzhaigou river water was also calculated by the three-component mixing model. The contribution of three sources could be estimated using the following equation:

$$Q_s = Q_g + Q_p + Q_l \quad (3)$$

$$Q_sC_s = Q_gC_g + Q_pC_p + Q_lC_l \quad (4)$$

$$Q_s\delta_s = Q_g\delta_g + Q_p\delta_p + Q_l\delta_l \quad (5)$$

where Q is the discharge and C and δ are the concentrations of the $\delta^{18}O$ and TDS, respectively. Subscripts s, g, p, and l refer to stream, groundwater, precipitation, and lake water, respectively. A suitable tracer choice to explain the hydrologic changes in discharge during a storm, as well as to identify dominant sources in the catchment, has become increasingly important [42]. Environmental tracers such as ^{18}O, ^{2}H, and excess deuterium, as well as geochemical data such as TDS, Electrical conductivity (EC), Cl, and SiO_2, are effective [43–46]. TDS and $\delta^{18}O$ were chosen as the conservative tracers in this study.

A classical Gaussian error propagation technique is useful to quantify the uncertainty of isotope hydrograph separations [47,48]. The relative error ω of the contribution of a specific runoff component is related to the uncertainty in each of the variables by the following:

$$\omega_y = \sqrt{\left(\frac{\partial y}{\partial x_1}\omega_{x1}\right)^2 + \left(\frac{\partial y}{\partial x_2}\omega_{x2}\right)^2 + \cdots + \left(\frac{\partial y}{\partial x_n}\omega_{xn}\right)^2} \quad (6)$$

where ω represents the uncertainty in the variable specified in the subscript. Errors of all separation equation variables were considered in this study. Uncertainties were caused by tracer analysis, as well as the discharge measurement and variability of ^{18}O.

3.3. ^{222}Rn Mass-Balance Model

^{222}Rn, produced by the decay of ^{226}Ra, is an inert radioactive gas with a half-life of 3.83 days. It has great potential to identify the rapid exchange processes of groundwater and surface water that occur on time scales of hours and days. In general, groundwater has ^{222}Rn concentration values of 2–3 times higher than surface water [49]. This difference can provide some information to estimate the percentage of groundwater inflow between two locations along a river. Based on the ^{222}Rn mass conservation theory [50], a ^{222}Rn mass-balance model was constructed in the Jiuzhaigou river. By taking the gas exchange and radioactive decay of ^{222}Rn in both river and groundwater discharge into account, the model can be expressed as follows [11,12,51]:

$$Rn_d = Rn_{gw}\cdot\frac{1-\exp(-\alpha\cdot L)}{L\cdot\alpha}\cdot\frac{Q_{gw}}{Q_r} + Rn_u\cdot\exp(-\alpha\cdot L)\cdot\left(1-\frac{Q_{gw}}{Q_r}\right) \quad (7)$$

$$\alpha = \frac{\lambda}{v} + \frac{D^{0.5}}{v^{0.5}\cdot h^{1.5}} \quad (8)$$

$$-LogD = 980/T + 1.59 \quad (9)$$

where Rn_d, Rn_u, and Rn_{gw} are ^{222}Rn concentrations measured in the downstream, upstream river, and groundwater, respectively (Bq/m^3); Q_r and Q_{gw} are river and groundwater discharge, respectively (m^3/s); α is the ^{222}Rn loss coefficient caused by both radioactive decay and gas exchange for the gas exchange part; L is the length between two stream sampling sites (m); v is the average stream velocity between two stream sampling sites (m/s); h is the stream depth (m); λ is ^{222}Rn radioactive decay coefficient (λ = 2.08 × 10^6 s^{-1}); D is radon molecular diffusivity (cm^2/s); $-Log\ D$ = (980/T) + 1.59; and T is absolute water temperature (K). Thus, the groundwater proportion in river discharge (Q_{gw}/Q_r) could be calculated by solving the equation.

According to the hydrogeological conditions and streamflow measurements of hydrologic stations, the typical methods for quantifying groundwater fluxes and exchange with river water in the Jiuzhaigou were conducted. The mass balance method to estimate specific transformations between groundwater and river water along a detailed section at two sampling sites was employed [12].

Assuming that groundwater discharge into the river, $Rn_d > Rn_u$, $Q_d > Q_u$, where q_g is the average groundwater fluxes for the entire width and per length of the river (m^3/(s·m)):

$$Rn_d \cdot Q_d = \int_0^l q_g Rn_{gw} \cdot \exp(-\alpha \cdot x)dx + Rn_u \cdot \exp(-\alpha \cdot L) \cdot Q_u \tag{10}$$

$$q_g = \frac{Rn_d \cdot Q_d - Rn_u \cdot \exp(-\alpha \cdot L) \cdot Q_u}{Rn_{gw}} \cdot \frac{\alpha}{1 - \exp(-\alpha \cdot L)} \tag{11}$$

Assuming that river discharges into groundwater when $Rn_d < Rn_u$ and $Q_d < Q_u$, where q_r is the average river leakage for the entire width and per length of the river (m^3/(s·m)):

$$Rn_d \cdot Q_d = Rn_u \cdot \exp(-\alpha \cdot L) \cdot Q_u - \int_0^l q_r Rn_u \cdot \exp(-\alpha \cdot (L - x))dx \tag{12}$$

$$q_r = \frac{Rn_d \cdot Q_d - Rn_u \cdot \exp(-\alpha \cdot L) \cdot Q_u}{Rn_u} \cdot \frac{\alpha}{\exp(-\alpha \cdot L) - 1} \tag{13}$$

Assuming that two processes both occur including groundwater discharge and river leakage when $Rn_d < Rn_u$ and $Q_d > Q_u$:

$$Rn_d \cdot Q_d = \int_0^l q_g Rn_{gw} \cdot \exp(-\alpha \cdot x)dx + Rn_u \cdot \exp(-\alpha \cdot L) \cdot Q_u - \int_0^l q_r \frac{(Rn_u + Rn_d)}{2} \cdot \exp(-\alpha \cdot (L - x))dx \tag{14}$$

$$Q_d = Q_u + q_g L - q_r L \tag{15}$$

$$q_r = \frac{2\alpha(Rn_d \cdot Q_d - Q_u Rn_u \cdot \exp(-\alpha \cdot L))}{(1 - \exp(-\alpha \cdot L))(2Rn_{gw} - Rn_u - Rn_d)} - \frac{2Rn_{gw}(Rn_d - Rn_u)}{L(2Rn_{gw} - Rn_u - Rn_d)} \tag{16}$$

$$q_g = \frac{2\alpha(Rn_d \cdot Q_d - Q_u Rn_u \cdot \exp(-\alpha \cdot L))}{(1 - \exp(-\alpha \cdot L))(2Rn_{gw} - Rn_u - Rn_d)} - \frac{(Rn_{gw} + Rn_d)(Rn_d - Rn_u)}{L(2Rn_{gw} - Rn_u - Rn_d)} \tag{17}$$

4. Results

4.1. Regional Surface Water Level and Streamflow Change

Figure 3a shows water level variations of all the monitoring stations before and after the earthquake in a month. In the ZCW valley, the water level of Changhai Lake and Colorful Pond decreased synchronously after the earthquake despite increased precipitation amount for a month until September 2017, indicating that Colorful Pond was connected with Changhai Lake. Gradually, Changhai Lake's water level fell by 0.8 m in a month, the seepage of which was about 870,000 cubic meters as a recharging resource due to the earthquake. This water level drop lasted for more than a month after the earthquake and eventually recovered to rise again.

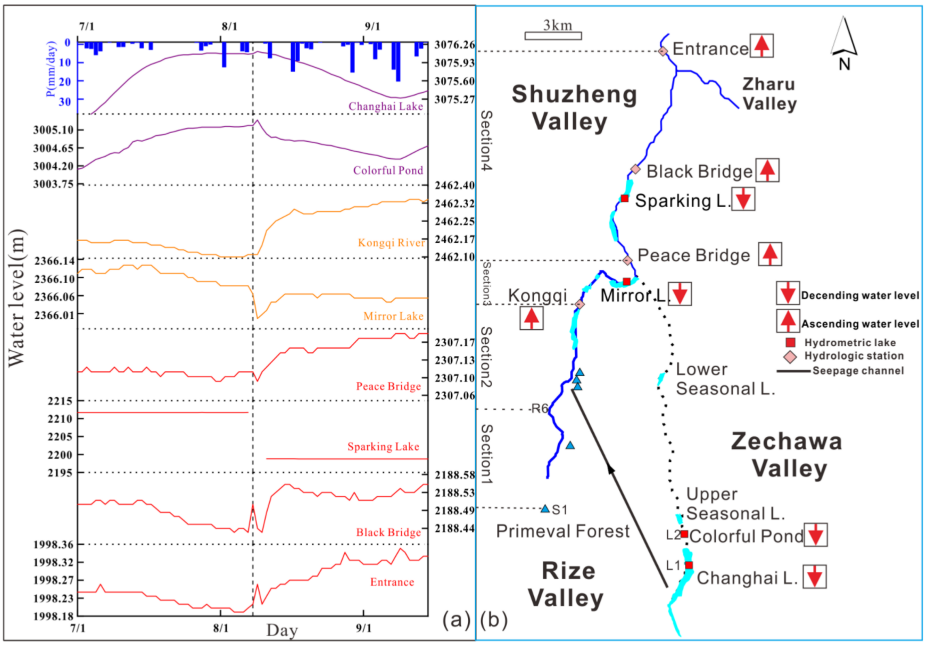

Figure 3. (**a**) Water levels of four hydrometric lakes and four hydrologic stations in three valleys. (**b**) Regional water level changes induced by the earthquake. The dashed black line represents the Mw6.5 earthquake, and the blue column refers to the amount of precipitation. The water level data are presented in Table S1 of the Electronic Supplementary Materials (ESM).

In the RZ valley, Kongqi River had an incremental recovery of water level. The western river could be recharged from Changhai Lake water. The underflow groundwater flowed into the RZ river through the seepage channel from Changhai Lake, as shown in Figure 3b. On the contrary, the sharp decline of Mirror Lake's water level as a co-seismic response reached 6 cm and returned to approximately the prestimulated value. Additionally, ground fissures had been produced on a road near Mirror Lake (as found during field observation), and the surface cracking and shedding appeared in the core landscape of Nuorilang Waterfall. It was predicted that new bedrock fractures were produced near the ruptured fault.

In the SZ valley, the Peace Bridge water level had a slight decrease due to Mirror Lake leakage or Nuorilang Waterfall cracking, both of which were upstream. Then, the Peace Bridge water level increased and sustained. A sharp decline of Sparking Lake's water level from 2212 to 2197 m was caused by the Sparking Lake dam-break induced by the earthquake. The water levels of the entrance and Black Bridge both had abrupt increases due to 450,000 cubic meters of lake water loss and a 15-m drop of Sparking Lake. One month before the earthquake, the water level of Kongqi River, Black Bridge, and the entrance showed a falling tendency, while that of Changhai Lake slowly arose. Another month after the earthquake, the lake water level of the ZCW valley in the east decreased. However, the river water level of the RZ valley in the west increased (Figure 3b). This indicated that Changhai Lake water from the ZCW valley in the east possibly discharged into the RZ valley in the west via the seepage channel.

Figure 4 shows the streamflow variations of four hydrologic stations in the SZ and RZ rivers before and after the earthquake in 2017. The annual average discharge volumes of the entrance, Black Bridge, Peace Bridge, and Kongqi River were 11.28, 11.22, 5.14, and 4.82 m^3/s, respectively. Additionally, the annual average discharge was 11.28 m^3/s in the SZ trunk river and 4.82 m^3/s in the RZ river. Therefore, the discharge from the ZCW valley was 6.46 m^3/s, based on Equation (1). The SZ trunk was recharged by 57% from the ZCW valley, and 43% from the RZ river according to the actual discharge volume calculation.

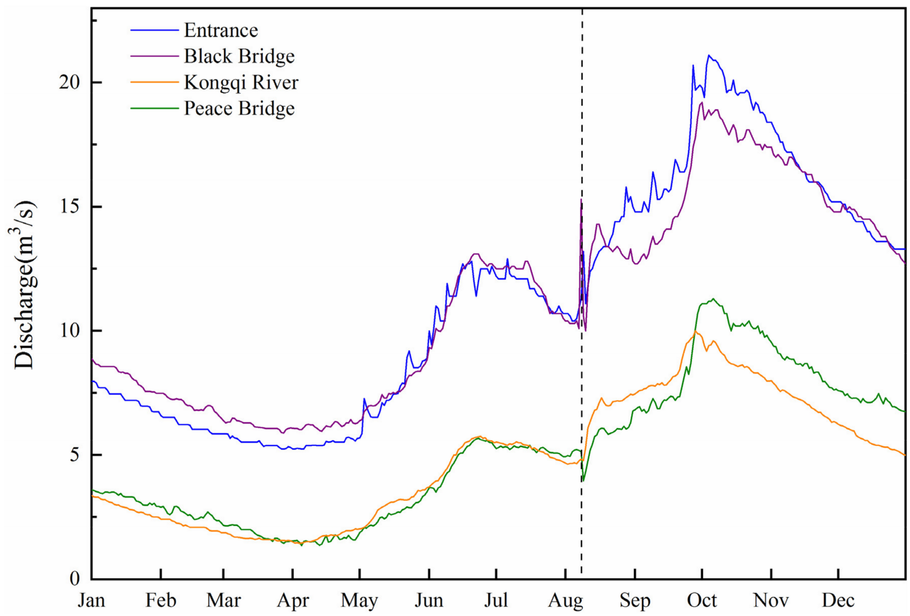

Figure 4. Hydrographs of four hydrologic stations in the Rize (RZ) and Shuzheng (SZ) rivers in 2017. The dashed black line represents the Mw6.5 earthquake. The discharge data are presented in Table S1 of the ESM.

4.2. Hydrochemical Characteristics

The water in Jiuzhaigou is divided into three categories: springs, river water in the RZ and SZ valleys, and lakes in the ZCW valley, according to the chemistry characteristic and sampling location (Table 1). A Piper plot is shown in Figure 5. The surface water (river and lake) type was found to be HCO_3–Ca–Mg. In the river, the major cation is Ca and ranges in concentration from 38.7 to 59.8 mg/L, Mg concentration ranges from 10.5 to 15.2 mg/L, pH varies from 8.0 to 10.2, and TDS ranges from 160.6 to 218.6 mg/L. Lakes in the ZCW valley have the lowest concentration Ca of 34.6–37.7 mg/L, Mg of 9.6–10.1 mg/L, and TDS of 141.0–155.6 mg/L. The pH of lake water ranges from 8.31 to 8.56. The water chemistry types of springs include HCO_3–Ca–Mg, HCO_3–SO_4–Ca–Mg, and HCO_3–Ca. The concentration of Ca in the springs ranges from 32.0 to 118.1 mg/L, the concentration of Mg ranges from 7.4 to 33.7 mg/L, pH ranges from 7.1 to 8.5, and TDS ranges from 119.1 to 409.1 mg/L. The RZ spring, S5, has the highest concentration Ca^{2+} of 118.1 mg/L and a TDS of 409.1 mg/L, which has the water type of HCO_3–Ca.

Table 1. Field parameters, major ions, and water isotopes.

Type	Sample ID	Valley	Distance [a]	Altitude	T	pH	Na	K	Mg	Ca	F	Cl	HCO_3	SO_4	TDS	$\delta^{18}O$	$\delta^{2}H$	^{222}Rn	^{222}Rn Error
			(km)	(m)	°C		mg/L	mg/L	mg/L	mg/L	mg/L	mg/L	mg/L	mg/L	mg/L	‰	‰	(Bq/m^3)	(Bq/m^3)
River	R1	RZ	27.65	2980	6.9	8.0	0.0	0.3	10.5	46.6	0.3	1.7	21.6	179.9	171.0	−12.8	−89.6	35,765	3813
	R2	RZ	27.17	2942	7.2	8.4	0.0	0.3	10.5	44.5	0.4	1.7	23.6	172.2	167.0	−12.8	−89.5	7234	4125
	R3	RZ	25.86	2954	6.8	8.3	0.0	0.3	10.9	44.3	0.4	1.7	23.7	172.2	167.3	−13.0	−88.7	3650	1800
	R4	RZ	25.09	2900	15.2	8.4	0.0	0.3	11.0	44.6	0.4	1.8	23.6	174.8	169.0	−12.8	−88.3	4334	1402
	R5	RZ	25.10	2900	15.2	8.3	0.0	0.3	8.8	46.1	0.4	1.8	23.4	167.8	164.7	−12.9	−88.4	3214	1235
	R6	RZ	22.87	2760	8.2	10.2	0.0	0.3	10.9	43.9	0.4	1.6	23.5	174.0	167.6	−13.0	−89.5	1587	610
	R7	RZ	21.68	2601	7.1	8.3	0.0	0.3	10.8	43.9	0.4	1.7	23.4	170.1	165.5	−12.9	−88.4	3002	1578
	R8	RZ	20.48	2645	7.6	8.3	0.3	0.4	13.1	59.8	0.5	2.3	25.6	233.1	218.6	−12.8	−87.3	3627	2115
	R9	RZ	16.56	2476	12.5	8.3	0.3	0.4	12.7	50.2	0.4	1.1	24.2	200.4	189.6	−12.7	−86.9	8053	3576
	R10	RZ	15.69	2477	11.5	8.2	0.6	0.5	14.2	55.7	0.6	2.4	25.8	226.1	212.8	−12.6	−85.9	11,256	1100
	R11	RZ	13.10	2306	10.1	8.2	0.7	2.2	15.2	53.1	0.6	3.7	25.7	226.0	214.1	−12.6	−85.7	1101	735
	R12	RZ	12.88	2272	9.8	8.4	0.4	0.4	13.5	44.3	0.5	1.9	24.6	178.2	174.8	−12.2	−83.7	1637	1093
	R13	RZ	12.73	2322	9	8.3	0.3	0.4	12.8	38.7	0.4	1.8	23.3	165.8	160.6	−12.1	−81.2	7412	2441
	R14	SZ	12.13	2314	9.3	8.1	0.5	0.5	14.5	48.4	0.4	1.0	24.7	207.9	194.0	−12.3	−84.6	10,657	2046
	R15	SZ	7.70	2207	11.2	8.3	0.6	0.5	14.7	44.8	0.5	1.1	25.4	195.1	185.1	−12.4	−84.6	3716	1601
	R16	SZ	6.78	2188	14.3	8.5	0.6	0.5	14.8	44.6	0.4	0.9	29.5	195.2	188.9	−12.4	−84.2	2214	1350
	R17	SZ	0.00	2004	11.8	8.5	0.7	0.5	12.1	42.9	0.4	1.0	28.5	170.1	171.1	−12.2	−82.9	1400	991
Spring	S1	RZ	27.87	2960	6.8	7.9	0.0	0.3	10.4	46.7	0.3	1.7	21.9	182.5	172.5	−13.1	−90.3	5365	2626
	S2	RZ	26.76	3012	8.7	8.5	0.0	0.4	20.1	34.3	0.6	0.4	68.3	100.2	174.2	−12.5	−86.1	693	460
	S3	RZ	21.28	2700	8.2	7.7	0.3	0.5	13.3	63.9	0.6	2.3	25.1	246.9	229.5	−12.7	−87.7	12,702	5068
	S4	RZ	21.30	2690	8.8	7.4	0.9	0.6	17.0	86.1	0.8	3.1	30.4	340.4	309.0	−12.7	−87.6	15,516	4893
	S5	RZ	21.59	2675	10.6	7.1	0.0	1.1	12.6	118.1	0.9	2.5	35.0	477.6	409.1	−12.7	−86.1	25,481	4681
	S6	RZ	16.30	2547	11.2	7.9	0.8	0.5	15.5	58.7	0.6	2.4	26.7	245.2	227.8	−12.6	−86.4	12,804	3744
	S7	RZ	15.50	2460	8.6	8.3	5.0	2.7	33.7	78.4	0.5	8.5	103.9	274.6	370.0	−10.1	−67.9	178	358
	S8	SZ	10.30	2304	9.5	8.3	0.7	0.5	23.9	50.4	0.6	1.1	25.7	251.5	228.5	−12.0	−80.7	2610	1063
	S9	SZ	8.61	2263	10.4	8.3	0.6	0.5	14.7	46.0	0.5	1.0	25.1	200.2	188.5	−12.4	−84.5	1520	825
	S10	SZ	7.85	2195	10.9	8.3	0.6	1.2	14.6	44.0	0.4	1.7	27.9	187.4	184.2	−12.4	−84.4	2855	1717
	S11	SZ	6.87	2210	10	8.5	0.2	0.2	10.6	36.8	0.3	0.6	24.6	150.1	148.5	−12.3	−82.4	14,430	2277
Lake	L1	ZCW	28.64	2984	9.6	8.6	0.0	0.3	9.8	34.9	0.3	1.5	24.8	134.7	139.0	−12.1	−82.5	9143	624
	L2	ZCW	26.61	2911	8.1	8.3	0.0	0.3	10.1	34.6	0.3	0.7	25.7	135.1	139.3	−12.2	−82.9	-	-
	L3	ZCW	26.85	2933	6.2	8.3	0.2	0.4	11.8	37.9	0.5	0.8	25.7	154.0	154.2	−12.2	−83.5	-	-
	L4	ZCW	18.76	2604	10.5	8.6	0.1	0.4	9.6	37.7	0.4	0.8	23.6	147.0	146.1	−12.2	−82.9	18,539	2748

[a] The distance is the direct distance away from the location of R17.

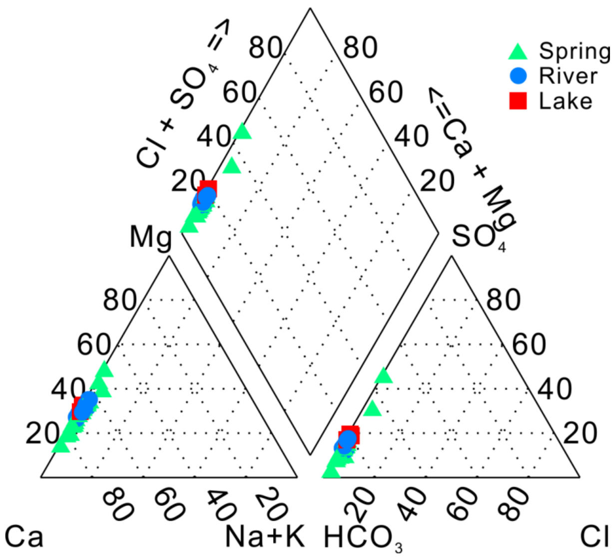

Figure 5. Piper diagram of the spring, river, and lake water samples; percentage concentrations in meq/L.

4.3. Stable Isotopic Compositions of Hydrogen (δ^2H) and Oxygen ($\delta^{18}O$)

The stable isotopic compositions ($\delta^{18}O$ and δ^2H) of the water samples in the study area were shown in Figure 6 and Tables 1 and 2. The local meteoric water line (LMWL) for the Jiuzhaigou catchments was established as $\delta^2H = 8.38 \times \delta^{18}O + 20$, ($R^2 = 0.97$, $n = 31$), based on the precipitation sampled weekly at the Changhai Lake precipitation station. The slope and intercept of the LMWL were found to be higher than the slope (8) and intercept (10) of the Global Meteoric Water Line (GMWL; $\delta^2H = 8 \times \delta^{18}O + 10$) [52]. The equation for LMWL was similar to the regional meteoric water line for the Tibetan plateau ($\delta^2H = 8.41 \times \delta^{18}O + 16.72$) [53].

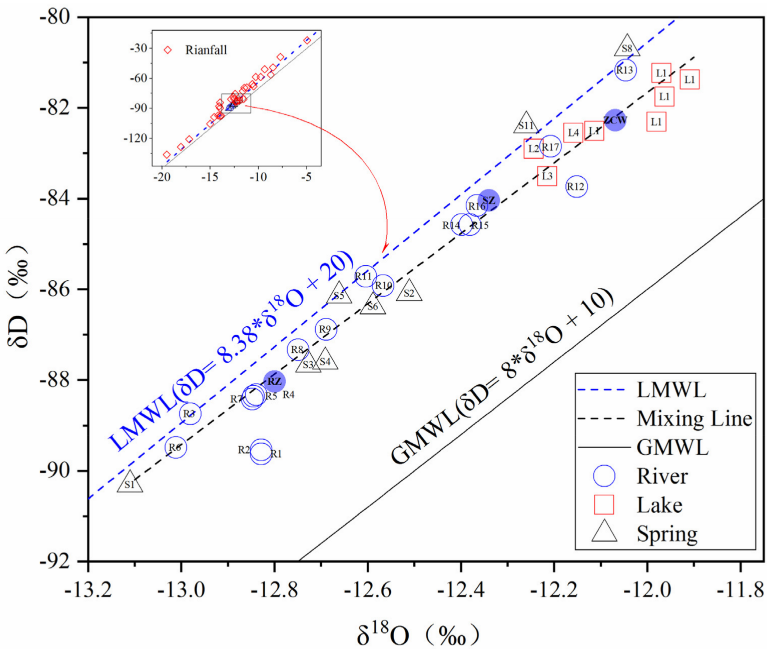

Figure 6. Stable isotopes of rainfall, spring, lake, and river water in Jiuzhaigou. The solid circle represents the isotopic average value of three valleys. Changhai Lake (L1) water was sampled many times.

Table 2. $\delta^{18}O$ and $\delta^{2}H$ isotopes of precipitation at the Changhai Lake precipitation station.

Type	No	Sample ID	Date (yy/mm/dd)	Amount (mm)	$\delta^{18}O$‰	δD‰
Rain	1	CH-01	2019/10/23	17.5	−14.0	−89.8
Rain	2	CH-02	2019/10/30	40	−19.5	−136.3
Rain	3	CH-03	2019/11/7	23.1	−17.2	−120.8
Rain	4	CH-04	2019/11/14	1.8	−11.2	−69.2
Rain	5	CH-05	2019/11/20	2.2	−12.8	−80.8
Rain	6	CH-06	2019/11/28	2	−9.8	−58.5
Rain	7	CH-07	2019/12/19	12.5	−12.6	−78.4
Snow	8	CH-08	2019/12/26	1.6	−10.3	−58.5
Snow	9	CH-09	2020/1/9	1.8	−14.0	−97.7
Snow	10	CH-10	2020/1/17	2.6	−13.9	−97.3
Snow	11	CH-11	2020/1/23	4.3	−14.2	−97.1
Snow	12	CH-12	2020/1/31	2.5	−14.6	−98.5
Snow	13	CH-13	2020/2/6	5.5	−14.1	−87.9
Snow	14	CH-14	2020/2/13	2.5	−12.4	−75.6
Snow	15	CH-15	2020/2/20	2.1	−14.0	−84.3
Snow	16	CH-16	2020/2/26	0.7	−8.5	−49.0
Snow	17	CH-17	2020/3/5	11.2	−12.5	−80.5
Snow	18	CH-18	2020/3/12	15	−11.6	−72.6
Rain	19	CH-19	2020/3/19	17.3	−10.7	−65.7
Rain	20	CH-20	2020/3/26	13.2	−11.5	−69.4
Rain	21	CH-21	2020/4/2	19.5	−9.4	−50.8
Rain	22	CH-22	2020/4/9	46	−18.0	−128.7
Rain	23	CH-23	2020/4/16	10.2	−7.7	−38.7
Rain	24	CH-24	2020/4/23	29.4	−15.0	−105.3
Rain	25	CH-25	2020/5/7	6.6	−4.9	−21.9
Rain	26	CH-26	2020/5/14	27.4	−10.5	−67.8
Rain	27	CH-27	2020/5/21	24.2	−12.4	−83.4
Rain	28	CH-28	2020/5/28	31.2	−12.3	−83.4
Rain	29	CH-29	2020/6/4	21.6	−12.3	−83.4
Rain	30	CH-30	2020/6/11	21.1	−8.7	−56.6
Rain	31	CH-31	2020/6/18	38.6	−11.6	−80.6

CH: Changhai.

The different water types in Jiuzhaigou showed distinct isotopic compositions, as seen in Figure 4. (i) Rainfall samples were found to have a wide range from −19.5‰ to −4.9‰ of $\delta^{18}O$ and from −136.3‰ to −21.9‰ of $\delta^{2}H$. (ii) ZCW lakes (L1–L4) were found to be enriched in $\delta^{18}O$ and $\delta^{2}H$ isotopes with a range from −12.2‰ to −11.9‰ and −83.5‰ to −81.4‰, respectively, while RZ river water had the same altitude, with $\delta^{2}H$ ranging from −88.9 to −85.4‰ and $\delta^{18}O$ from −13.1 to −12.5‰. Changhai Lake (L1) was located at the highest altitude, but $\delta^{2}H$ and $\delta^{18}O$ in the ZCW lake were found to be the most enriched and were plotted in the top-right of the LMWL, which indicated an evaporation effect [38]. (iii) The $\delta^{2}H$ and $\delta^{18}O$ water levels in three valleys were found to follow the ranking of ZCW > SZ > RZ, and the average $\delta^{18}O$ values were found to be −12.0‰, −12.3‰, and −12.8‰, respectively. Additionally, the average $\delta^{2}H$ values were found to be about −82‰, −84‰, and −88‰, respectively. The isotope level of the SZ samples was between those of the RZ and ZCW water isotopes, indicating a mixing effect. The contributions of ZCW and RZ water in the SZ river were found to be 62 ± 19% and 38 ± 19%, respectively, based on two-component isotope hydrograph separation (Equations (1), (2), and (6)). The results were the consistent with the fractions calculated by the actual discharge volume. A mixing line ($\delta^{2}H = 7.76 \times \delta^{18}O + 11.46$) was obtained, and its slope was lower than the 8 of the GMWL slope. This indicated surface water evaporation. Most spring samples (S2, S3, S4, and S6) fell on the mixing line, indicating that they were recharged by Changhai Lake water. Therefore, the water connectivity of ZCW and RZ existed. (iv) Our field investigation showed that the original upstream source of the RZ river was a spring; This was the S1 sample. S1 was found to fall on the LMWL with the most depleted isotope value, which was related to the higher recharging altitude from precipitation. S8 and S11 were found to fall on the LMWL with an enriched isotope level related to the lower recharging altitude. R12 and R13, which were sampled at the intersection of the RZ and ZCW valleys (Figure 6), were found to have similar isotopic compositions to that of Changhai Lake. This indicated that they directly replenished from Changhai Lake water.

Along the river stretch, the $\delta^{18}O$ value of water was found to have an increasing trend from S1 to R17 (Figure 7). Two flow pathways could be identified. Path 1 is the main water connectivity path between Changhai Lake and the RZ upstream river. Springs (S2–S5) are the outcrops of groundwater, as Changhai Lake water discharges into the RZ valley across the surface watershed. Path 2 is different water connectivity path between Changhai Lake and the downstream RZ river. R12, R13, S8, and S11 can be considered as the underflow groundwater sites of Changhai Lake, though the ZCW valley is a dry valley on the surface. ZCW and RZ water flow into the SZ river together at the intersection of two branches.

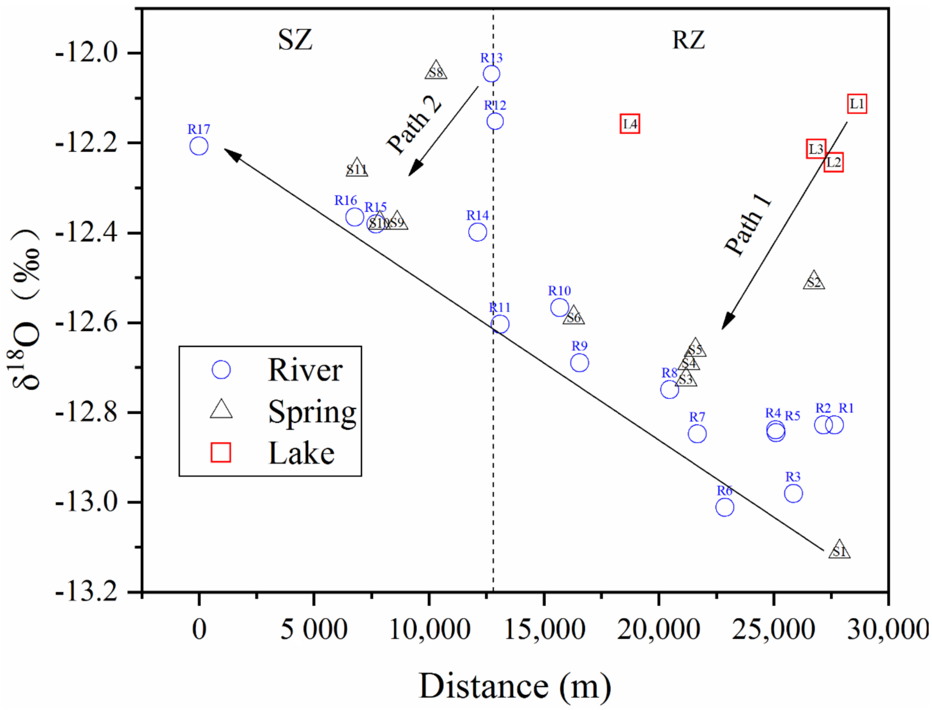

Figure 7. $\delta^{18}O$ changes of water samples along three valleys.

4.4. *Tritium (^3H) of River, Lakes and Springs*

The tritium contents of the ZCW lakes (L1, L2, and L3) were found to be 12.5, 13.7, and 13.1 TU, respectively. The average was 13.1 ± 0.6 TU, approximately representing the tritium in precipitation. In the RZ valley, the tritium contents of springs (S1, S5, and S7) were found to be 11.7, 10.2, and 9.4 TU, respectively. S7, a groundwater member, was found to have the lowest tritium content of 9.4 ± 0.4 TU, which means that it is relatively "old" site of groundwater replenishment with a lower tritium concentration injunction between the ZCW and RZ valleys as a drainage area. The average tritium content of water samples (S10 and R15) that are exposed the bottom of Sparking Lake due to the dam break in the SZ river was found to be 10.4 ± 0.3 TU. Based on Equations (1), (2), and (6), the contributions of precipitation and groundwater in the SZ river water were found to be 27 ± 12% and 73 ± 12%, respectively. Tritium, the radioactive isotope of hydrogen of mass three with a half-life of 12.43 years, has served as an important and useful tracer to determine recent groundwater recharge, movement, and residence times for surface water and groundwater in hydrological studies [54,55]. The tritium sequence in Chengdu station from Global Network of Isotopes in Precipitation (GNIP) near the Jiuzhaigou area from 1986 to 1998 was used in this study. Based on the principle of radioactive decay, the precipitation of tritium for 2019, which represented the tritium that had infiltrated the groundwater between 1986 and 1998, was calculated in Figure 8. ^{3}H contents in Jiuzhaigou showed that groundwater had a short residence time and it was a moderate precipitation. Changhai Lake water had the highest tritium content of more than 10 TU. The higher tritium values were caused by the recycling of moisture evaporated from the lake surface without outflow. It still had a considerable amount of tritium deposited during thermonuclear tests in this region [56].

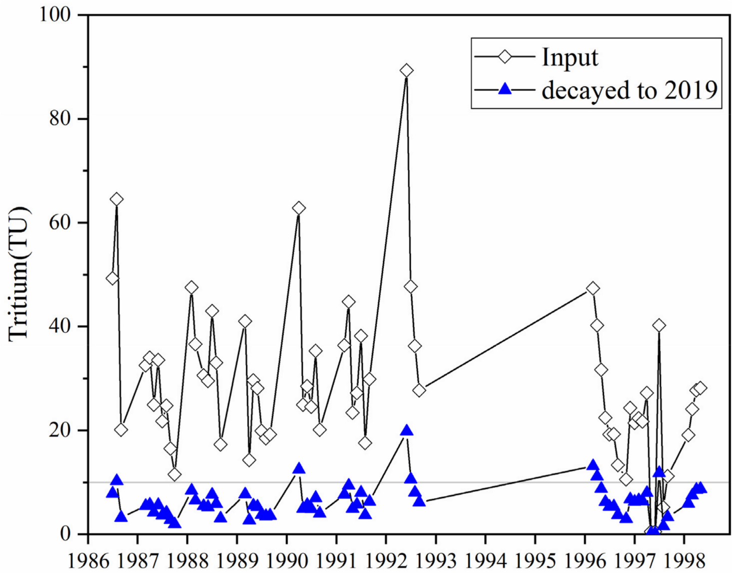

Figure 8. The tritium precipitation input from 1986 to 1998 and the decayed tritium precipitation content as of 2019 (data from GNIP Chengdu station).

4.5. ^{222}Rn Concentrations in River and Spring

^{222}Rn concentration in the rivers and springs showed a wide scale that ranged from 1101 to 35,765 Bq/m^3. These concentrations were found to be about 1101–35,765 and 2320–25,481 Bq/m^3 for samples of the rivers and springs, respectively. Additionally, the average ^{222}Rn concentrations were found to be about 6462 and 7770 Bq/m^3 for the samples of the rivers and springs, respectively. The distribution of the ^{222}Rn concentrations is shown in Figure 9 and Table 1.

Four sections were divided along the river stretch according to the distributions and changes of ^{222}Rn concentration. Section 1 stretches from R1 to R6, located upstream of the RZ river. The ^{222}Rn isotope activity of river water was found to decrease significantly from 35,760 to 3210 Bq/m^3, indicating that the natural decay of ^{222}Rn isotope in this section had become the main controlling factor. Surface water was typically transformed into groundwater, and the stream discharge of R6 was found to be more than that of R1. Section 2 was found to have an increasing ^{222}Rn isotope activity. The S5 sample was found to have the highest ^{222}Rn concentration in the RZ valley, indicating that it can represent groundwater characteristics from the deep aquifer. From R6 to R10 along the flow path, the ^{222}Rn activity of the river water samples was found to generally increase from 1587 to 11,256 Bq/m^3, with an average value of 5505 Bq/m^3. For springs, it was found to decrease from 25,481 to 12,804 Bq/m^3, with an average value of 16,626 Bq/m^3. The ^{222}Rn concentration of groundwater was found to decrease along the river stretch, while the ^{222}Rn concentration of the river water was found to increase in this region. This indicated that the river water of this section was mainly formed by groundwater discharge. The river water got more ^{222}Rn from groundwater. Section 3 was found to have a decreasing trend of ^{222}Rn isotope activity from R10 to R11, while a significant increase was found from R11 to R14. This indicated that two processes of groundwater discharge and river leakage possibly occur within Section 3. In the SZ river, Section 4 was found to have the same variation trend of ^{222}Rn concentration as Section 1. From R14 to R17, the ^{222}Rn activity of the river water was found to decrease from 10,660 to 1400 Bq/m^3.

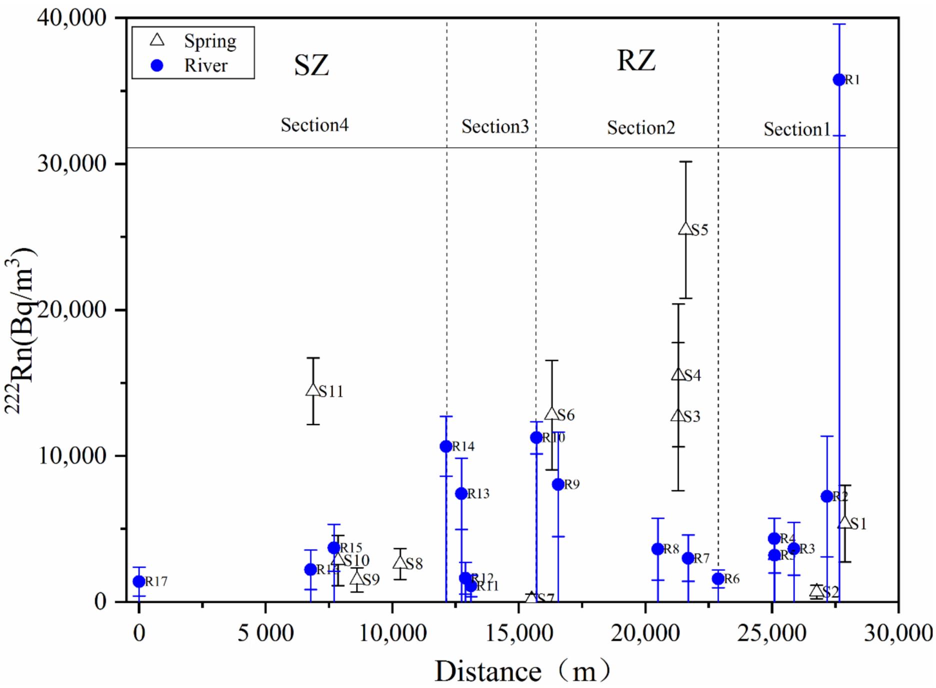

Figure 9. ^{222}Rn concentration changes of river water and springs along the RZ and SZ rivers. The error bars represent the standard deviation of all ^{222}Rn samples.

5. Discussion

5.1. Source Identification and Quantification of River Water

A three-component mixing model was used to estimate water flux along the RZ and SZ rivers. Precipitation, groundwater, and Changhai Lake water were the end-members for the model, forming the runoff discharge. The weighted isotopes of precipitation in Jiuzhaigou were found to be −13.3‰ for δ^{18}O and −88.9‰ for δ^2H. The rain TDS was considered as 20 mg/L. According to observations and measurements on the spring discharge, the RZ spring groups (S3, S4, and S5), exposed at the valley–fault intersection, have a relatively steady discharge volume of 1.4–1.7 m^3/s. S5, especially, has the highest TDS and ^{222}Rn concentration among these springs. During the sampling of S5 after the earthquake, an intense-smelling H_2S appeared. A considerable amount of H_2S rose along an active fault and dissolved into the groundwater. The high TDS was related to the water–rock interactions with a relatively deep groundwater circulation. Therefore, the S5 sample was considered to be a deeper groundwater member, with an δ^{18}O of −12.7‰ and a TDS of 409.1 mg/L. The Changhai Lake water was found to have the most enriched δ^{18}O of −12.1‰ as a lake member, with a TDS of 141.27 mg/L. The samples of precipitation, groundwater, and Changhai Lake formed a triangle to test and verify the independence of three end-members (Figure 10). Most river samples were found to fall into the triangle. However, R12, R13, S1, and S8 lie outside of the triangle. S1, the origin spring of the RZ river with the same altitude as Changhai Lake, was not recharged by Changhai Lake water. The groundwater can be easily transported when faults trend parallel or subparallel to the hydraulic gradient [57]. Therefore, water located at a low altitude was easily recharged from Changhai Lake. S8, S11, R12, and R13, which were close to L1, could be recharged from Changhai Lake water. Other outliers possibly resulted from uncertainty in field sampling and laboratory analyses or water source area changes [58,59].

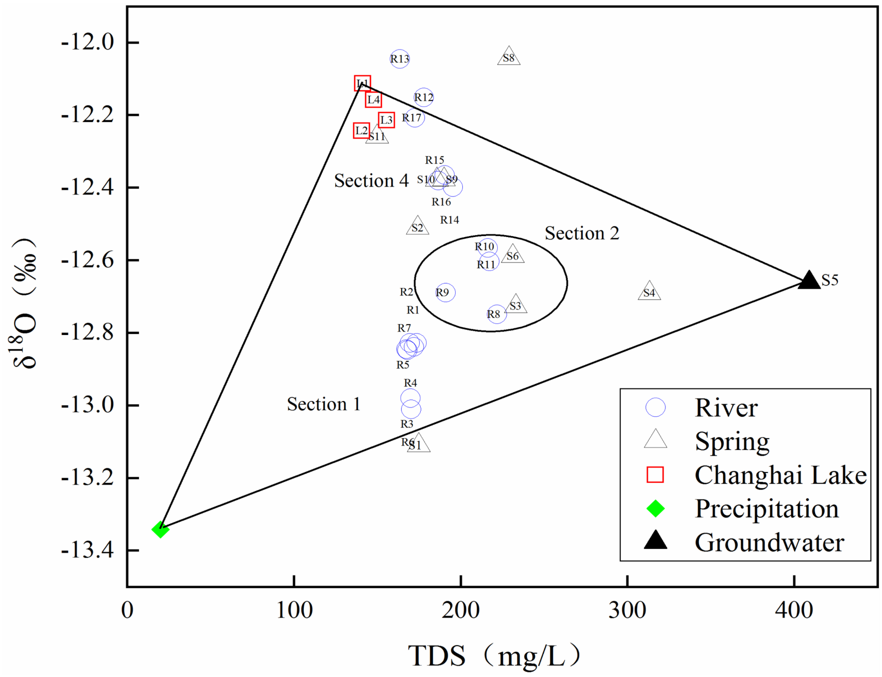

Figure 10. The average values of $\delta^{18}O$ and TDS of three end-members that form a triangle.

Due to the regional groundwater flow pathways, the surface runoff had three generating sources that had different hydrological characteristics and contributions. The results obtained based on Equations (3)–(5) were shown along the RZ and SZ rivers in Figure 11. In Section 1, the contribution of Changhai Lake water was found to be less than 20%. In Section 2, the fractions of Changhai Lake water in the river were found to begin to increase, as this was the main seepage area recharged by Changhai Lake. The average fractions of precipitation, groundwater, and Changhai Lake water in the RZ river were 33%, 36%, and 31%, respectively. Considering Changhai Lake's status as an underflow groundwater member, the average contributions of precipitation and groundwater in the river were found to be about 33% and 67%, respectively. This was also consistent with the result based on ^{3}H tracing methods. In Section 4, the contribution of Changhai Lake in the SZ river was more than 60%, which was consistent with the result of two-component isotope (^{18}O) hydrograph separation. This was because there was water connectivity between Changhai Lake and the RZ river.

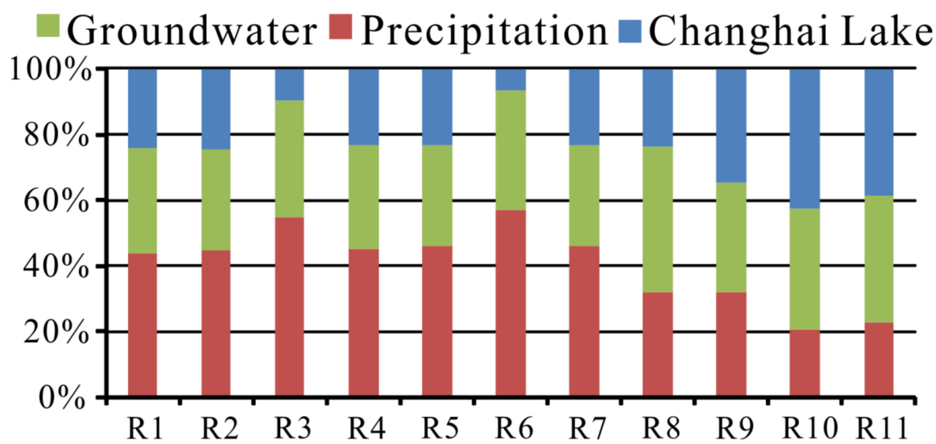

Figure 11. Estimated fraction of water sources as a result of hydrograph separation along the RZ river.

5.2. Estimation of Groundwater/River Water Interactions

A ^{222}Rn mass-balance model was constructed in four sections with river flow monitoring data to quantitatively calculate the river leakage, groundwater discharge, and proportion of groundwater in river discharge. During calculation, D was calculated to be 8.89×10^{10} m^2/s at 283.15 K (10 °C) from Equation (9), α was calculated to be 1.77×10^5 m^{-1} from Equation (8), Rn_{gw} was represented by the average ^{222}Rn concentration of springs in different sections, Q_u and Q_d were calculated by the observed average stream discharge of hydrological stations, and V and H were measured at the river cross sections of these stations during the sampling period. Groundwater was discharged into the river water (5.5 m^3/s for Q_{gw} and 69% for Q_{gw}/Q_r from Equation (7)) in Section 2 for about 7 km during the sampling period. The flux of groundwater discharge q_g was about 7.66×10^4 m^3/(s·m). The contribution of groundwater in the river was 69%. All of this was consistent with the result of isotope hydrograph separation.

In Section 1, Section 3, and Section 4 along the river stretch, the upstream ^{222}Rn concentration was more than the downstream concentration, while the upstream stream discharge was less than the downstream discharge. Two processes of groundwater discharge and river leakage occurred. The model parameters in these sections were substituted into Equations (16) and (17) (Table 3) to produce the results of groundwater discharge flux q_g and river leakage flux q_r: they were found to be 9.99×10^4 and 1.55×10^4 in Section 1, 11.1×10^4 and 8.39×10^4 in Section 3, and 9.19×10^4 and 1.02×10^4 m^3/(s.m) in Section 4, respectively; see in Table 3. The results showed that groundwater discharge plays a dominant role in these sections. Along the river stretch, the average groundwater discharge flux was found to be 9.47×10^4 m^3/(s.m), and the average river leakage flux was found to be 3.65×10^4 m^3/(s.m).

Table 3. Characteristics of the estimated sections and the calculated results obtained using the ^{222}Rn mass balance method.

Sections	Rn_u (Bq/L)	Rn_d (Bq/L)	Rn_{gw} (Bq/L)	Q_u (m^3/s)	Q_d (m^3/s)	V (m/s)	L (m)	H (m)	q_r m^3/(s*m)	q_g m^3/(s*m)
1	35.76	3.21	5.37	2.00	4.00	0.30	2549	1.50	1.55×10^4	9.99×10^4
2	1.59	11.26	16.63	5.85	8.32	1.07	7181	1.50	-	7.66×10^4
3	11.26	10.66	6.49	8.32	10.1	0.95	3565	1.25	8.39×10^4	11.1×10^4
4	10.66	1.40	5.35	10.1	18.9	1.11	12,127	1.30	1.02×10^4	9.19×10^4

It was expected that the transformation result between groundwater and surface water would be close to that obtained based on the flow balance. The ^{222}Rn model was validated by comparing it with the result of the flow balance method. The net exchange between groundwater and river represented the difference values of downstream and upstream discharges in each section from Equation (18). If it was a positive value, the downstream discharge exceeded the upstream discharge. This indicated river water was replenished from groundwater. Otherwise, a negative value meant that river water was lost and groundwater was recharged from river water. However, the flow balance method showed no detailed process in a different section, and this could be considered a reference to validate the ^{222}Rn model.

$$q = \frac{Q_d - Q_u}{L} \tag{18}$$

Results found with two methods were compared in Figure 12. As seen in Sections 1 and 4, the groundwater discharge flux q_g matched well with these two methods, and the calculated q_g with the ^{222}Rn method was about twice greater than that obtained with the flow balance method in Sections 2 and 3. The differences of results were still acceptable [12]. The uncertainties of estimation on groundwater discharge to the river resulted from the analysis errors of ^{222}Rn concentration in river water and groundwater, as well as the uncertainties from the manual measurement of stream parameters. Therefore, the water flux was validated by the ^{222}Rn mass balance method.

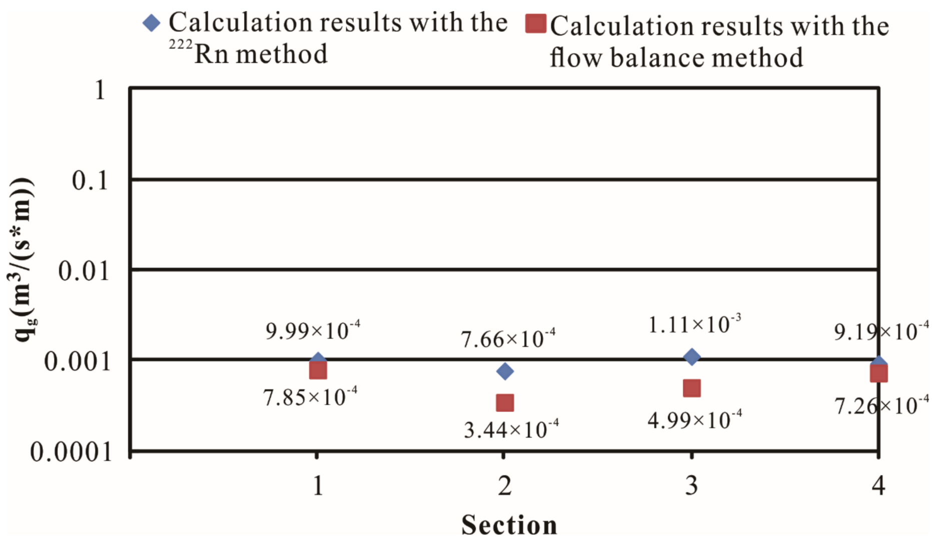

Figure 12. Comparison of calculated results of water flux using different methods.

5.3. Regional Groundwater Circulation Model

The conceptual model of three-dimensional water circulation was proposed in the study area (Figure 13). Jiuzhaigou valley was mainly composed of two tributaries and one trunk, including the RZ river in the west, the ZCW valley in the east, and the SZ river in the middle. The ZCW valley has perennial drought and four separate lakes. As the most important lake in the ZCW valley, Changhai Lake was recharged by precipitation and snow meltwater from surrounding high mountains. It was considered a slightly evaporated natural supply reservoir without a visible outlet. The Colorful Pond and upper and lower seasonal lakes in the ZCW valley had the same recharge altitude as Changhai Lake. They all belonged to seepage-type lakes with similar surroundings [60] that bear the same enriched isotope signatures due to evaporation. The S–N-oriented Jiuzhaigou and Zechawa Faults (F5 and F6, respectively) trended parallel or subparallel to the hydraulic gradient for water flow from south to north. They were conductive for groundwater transport. The surface water of the RZ river and ZCW valley tended to flow into the fault and out of the intersection, flowing into the SZ river together. The annual average discharges of the SZ and RZ rivers were 11.3 and 4.8 m^3/s, respectively. Therefore, the discharge of the ZCW valley into the SZ river was obtained as 6.5 m^3/s. Based on two-component isotope hydrograph separation, the two branches of the SZ trunk were recharged by 62 ± 19% from the ZCW valley and 38 ± 19% from the RZ river, consistent with the fractions calculated by the actual discharge volumes. The connectivity between Changhai Lake and the midstream RZ river was confirmed to exist across the local water divide according to the regional water level changes before and after the earthquake, water isotopic tracing analysis, and geological conditions. Based on the directly observed changes of regional water level for one month after the earthquake, the Changhai Lake water level decreased in the east, and the RZ river water level and discharge volume both increased in the west. Therefore, an underground hydraulic connection across the water divide was assumed between two branches. Regarding the useful confirmatory tracers, the $\delta^{18}O$ and δ^2H isotopes indicated that the RZ river water recharged from Changhai Lake water. The underground flow pathways were confirmed to exist. The cross-mountain faults (F3 and F4) may have been reactivated by the Jiuzhaigou earthquake. F3 and F4 near causative fault F1 acted as the important conduits to control the interbasin flow in the karstic catchments. Given that the high-permeability fault trended in the same direction as the hydraulic gradient, the fault normally had great effects on the groundwater flow [57]. Fault trends were good conductors with a relatively high transmissivity even for Changhai Lake water transport and discharge into the RZ river water across the water divide of a 4200-m mountain ridge. The water cycle system was sensitive to earthquake activities.

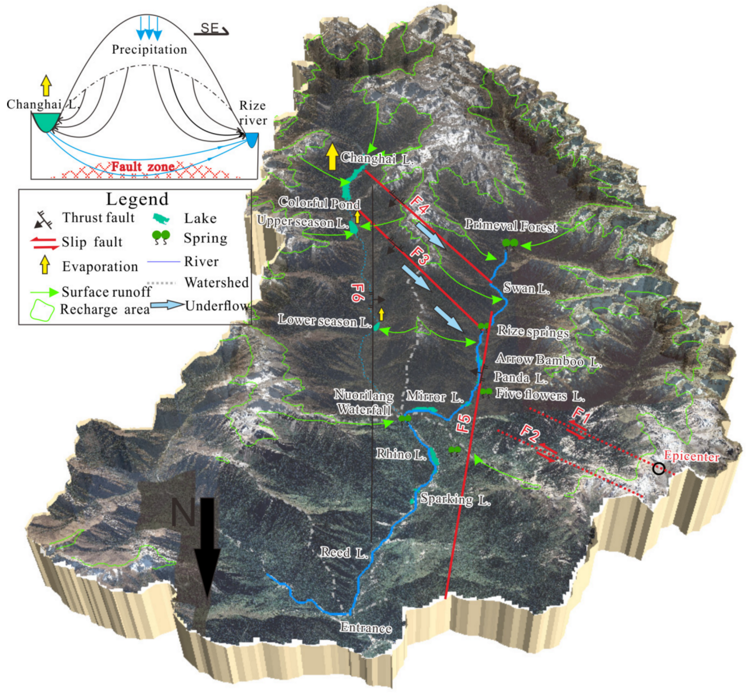

Figure 13. Schematic of conceptual model of three-dimensional post-earthquake water cycle. F1–6 represent faults shown in Figure 2a in detail.

Most springs were exposed at the valley–fault intersections with relatively high and steady flow rates, maintaining the perennial abundance of RZ river water. For example, the RZ spring group had a discharge volume of 1.4–1.7 m^3/s. It was exposed along the F3 fault that cut the major karst aquifer of the Carboniferous Minhe Group formation. Notably, it was found to have the highest TDS and ^{222}Rn concentration. An intense-smelling H_2S appeared in the spring vents after the earthquake. The high TDS concentration of the spring was related to the water–rock interactions with a relatively deep groundwater circulation. Therefore, the RZ spring was representative of deeper groundwater. Based on three-component isotope hydrograph separation, the RZ river was found to have been recharged by precipitation, groundwater, and Changhai Lake water. There were different fractions at the different river cross-sections, the averages of which were found to be 33%, 36%, and 31%, respectively. The source of the RZ river, a primeval forest spring, was precipitation. It was not recharged by Changhai Lake water. However, the midstream RZ river was the main discharging zone for Changhai Lake. The contribution of groundwater in the river was found to be 70% based on the ^{222}Rn mass balance model and the ^{3}H tracer. Most groundwater discharged into lakes and rivers via many springs from the recharge zone. Toruloid lakes along the RZ valley fed by springs were recharged by Changhai Lake. The springs were exposed at valley–fault intersections, with relatively high fracture-related permeability located in a fault damage zone. Groundwater was quickly driven and transmitted into surface water. The rapid interaction between surface water and groundwater was determined, thus allowing us to form a groundwater circulation model.

6. Conclusions

In this paper, we used multiple environmental isotope tracers (^{2}H, ^{18}O, ^{3}H, and ^{222}Rn) to discern the water cycle in the Jiuzhaigou catchments in the southeastern Tibetan Plateau. The regional water level changes over a month after the earthquake showed that the lake water level of the ZCW valley in the east had decreased and the water level of the RZ river in the west had increased. The water cycle system was found to be sensitive to earthquake activities due to the fact that there is a hydraulic connection underground across the water divide that controlled the distribution of surface flow in the two branches. A conceptual model of the water cycle was established by considering the contributions of different sources, including precipitation and groundwater, to the surface runoff. Based on isotope hydrograph separation, the surface water was found to have been recharged by precipitation, groundwater, and upper land lake (Changhai Lake) water; their fractions were 33%, 36%, and 31%, respectively, at the river outlet section. The water exchange direction and water flux between groundwater and surface water estimated using ^{222}Rn measurements indicated that 70% of the precipitation/surface water had undergone underground circulation, which demonstrated that well-developed surface vegetation made it easy for precipitation to recharge groundwater that eventually discharged into the river channel, a mechanism that optimal for maintaining the special waterscape.

The results showed that isotope tracers were effective in gauging the fractions of different water sources. Our study also implies that the regular monitoring of hydrological processes needs to be continued and enhanced in order to better formulate geo-hazard prevention and mitigation strategies for the world's natural heritage sites.

Supplementary Materials: The supplementary materials are available online at http://www.mdpi.com/2073-4441/12/12/3306/s1.

Author Contributions: Conceptualization, Z.P.; methodology, Z.P. and D.L.; field investigation, D.L., W.X., Y.H., J.D., G.S., and Z.P.; data handling, D.L., Y.H., and X.Y.; writing, review and editing, D.L. and Z.P. All authors have read and agreed to the published version of the manuscript.

Funding: This work was supported by the National Natural Science Foundation of China (NSFC Grant 41430319) and the World Natural Heritage Conservation and Restoration Research Program.

Acknowledgments: We gratefully acknowledge F.T. Yang for analyses of Radon isotopes. Thanks also go to Y.L. Kong and J. Li for discussions and useful suggestions on an earlier version of the manuscript. Our gratitude also goes to the Jiuzhaigou Disaster Recovery Project and World Natural Heritage Conservation and Restoration Research for their financial support.

Conflicts of Interest: The authors declare no conflict of interests.

References

1. Banks, E.; Simmons, C.T.; Love, A.J.; Shand, P. Assessing spatial and temporal connectivity between surface water and groundwater in a regional catchment: Implications for regional scale water quantity and quality. *J. Hydrol.* **2011**, *404*, 30–49. [CrossRef]
2. Sophocleous, M. Interactions between groundwater and surface water: The state of the science. *Hydrogeol. J.* **2002**, *10*, 52–67. [CrossRef]
3. Wang, W.; Dai, Z.; Zhao, Y.; Li, J.; Duan, L.; Wang, Z.; Zhu, L. A quantitative analysis of hydraulic interaction processes in stream-aquifer systems. *Sci. Rep.* **2016**, *6*, 19876. [CrossRef] [PubMed]
4. Woessner, W.W. Stream and fluvial plain ground water interactions: Rescaling hydrogeologic thought. *Ground Water* **2000**, *38*, 423–429. [CrossRef]
5. Zhu, L.; Gong, H.; Dai, Z.; Xu, T.; Su, X. An integrated assessment of the impact of precipitation and groundwater on vegetation growth in arid and semiarid areas. *Environ. Earth Sci.* **2015**, *74*, 5009–5021. [CrossRef]
6. Khadka, M.B.; Martin, J.B.; Kurz, M.J. Synoptic estimates of diffuse groundwater seepage to a spring-fed karst river at high spatial resolution using an automated radon measurement technique. *J. Hydrol.* **2017**, *544*, 86–96. [CrossRef]
7. Chapman, T.G. A comparison of algorithms for stream flow recession and baseflow separation. *Hydrol. Process.* **1999**, *13*, 701–714. [CrossRef]
8. Cook, P.G.; Favreau, G.; Dighton, J.C.; Tickell, S. Determining natural groundwater influx to a tropical river using radon, chlorofluorocarbons and ionic environmental tracers. *J. Hydrol.* **2003**, *277*, 74–88. [CrossRef]
9. Hatch, C.E.; Fisher, A.T.; Revenaugh, J.; Constantz, J.; Ruehl, C. Quantifying surface water–groundwater interactions using time series analysis of streambed thermal records: Method development. *Water Resour. Res.* **2006**, *42*. [CrossRef]
10. Kalbus, E.; Reinstorf, F.; Schirmer, M. Measuring methods for groundwater—Surface water interactions: A review. *Hydrol. Earth Syst. Sci.* **2006**, *10*, 873–887. [CrossRef]

11. Stellato, L.; Petrella, E.; Terrasi, F.; Belloni, P.; Belli, M.; Sansone, U.; Celico, F. Some limitations in using ^{222}Rn to assess river—Groundwater interactions: The case of Castel di Sangro alluvial plain (central Italy). *Hydrogeol. J.* **2008**, *16*, 701–712. [CrossRef]
12. Su, X.; Xu, W.; Yang, F.; Zhu, P. Using new mass balance methods to estimate gross surface water and groundwater exchange with naturally occurring tracer ^{222}Rn in data poor regions: A case study in northwest China. *Hydrol. Process.* **2015**, *29*, 979–990. [CrossRef]
13. Vespasiano, G.; Apollaro, C.; De Rosa, R.; Muto, F.; Larosa, S.; Fiebig, J.; Mulch, A.; Marini, L. The Small Spring Method (SSM) for the definition of stable isotope–elevation relationships in Northern Calabria (Southern Italy). *Appl. Geochem.* **2015**, *63*, 333–346. [CrossRef]
14. Vespasiano, G.; Cannata, C.; Cianflone, G.; Dominici, R.; Apollaro, C.; Rosa, R. Analysis of groundwater Pollution in the Sant'eufemia Plain (Calabria—South Italy). *Italian J. Eng. Geol. Environ.* **2016**, *16*. [CrossRef]
15. Apollaro, C.; Vespasiano, G.; De Rosa, R.; Marini, L. Use of mean residence time and flowrate of thermal waters to evaluate the volume of reservoir water contributing to the natural discharge and the related geothermal reservoir volume. Application to Northern Thailand hot springs. *Geothermics* **2015**, *58*, 62–74. [CrossRef]
16. Apollaro, C.; Vespasiano, G.; Muto, F.; De Rosa, R.; Barca, D.; Marini, L. Use of mean residence time of water, flowrate, and equilibrium temperature indicated by water geothermometers to rank geothermal resources. Application to the thermal water circuits of Northern Calabria. *J. Volcanol. Geotherm. Res.* **2016**, *328*, 147–158. [CrossRef]
17. Pang, Z.; Huang, T.; Chen, Y. Diminished groundwater recharge and circulation relative to degrading riparian vegetation in the middle Tarim River, Xinjiang Uygur, Western China. *Hydrol. Process.* **2010**, *24*, 147–159. [CrossRef]
18. Gordon, R.P.; Lautz, L.K.; Briggs, M.A.; Mckenzie, J.M. Automated calculation of vertical pore-water flux from field temperature time series using the VFLUX method and computer program. *J. Hydrol.* **2012**, *420*, 142–158. [CrossRef]
19. Xu, W.; Su, X.; Dai, Z.; Yang, F.; Zhu, P.; Huang, Y. Multi-tracer investigation of river and groundwater interactions: A case study in Nalenggele River basin, northwest China. *Hydrogeol. J.* **2017**, *25*, 2015–2029. [CrossRef]
20. Pang, Z.; Kong, Y.; Li, J.; Tian, J. An isotopic geoindicator in the hydrological cycle. *Procedia Earth Planet. Sci.* **2017**, *17*, 534–537. [CrossRef]
21. Clauer, N.; Techer, I.; Chaudhuri, S. Geochemical tracing of potential hydraulic connections between groundwater and run-off water in Northeastern Kansas, USA. *Hydrology* **2017**, *4*, 56. [CrossRef]
22. Hendry, M.J.; Schwartz, F.W. An alternative view on the origin of chemical and isotopic patterns in groundwater from the Milk River Aquifer, Canada. *Water Resour. Res.* **1988**, *24*, 1747–1763. [CrossRef]
23. Petitta, M.; Caschetto, M.; Galassi, D.M.P.; Aravena, R. Dual-flow in karst aquifers toward a steady discharge spring (Presciano, Central Italy): Influences on a subsurface groundwater dependent ecosystem and on changes related to post-earthquake hydrodynamics. *Environ. Earth Sci.* **2015**, *73*, 2609–2625. [CrossRef]
24. Qin, D.; Tao, S. Isotope constraints on the hydraulic relationship of ground-waters between Quaternary and Tertiary aquifer in Xi'an area; Shaanxi province. *Sci. China Ser. E Technol. Sci.* **2001**, *44*, 72–79. [CrossRef]
25. Hu, X.; Hu, K.; Tang, J.; You, Y.; Wu, C. Assessment of debris-flow potential dangers in the Jiuzhaigou Valley following the August 8, 2017, Jiuzhaigou earthquake, western China. *Eng. Geol.* **2019**, *256*, 57–66. [CrossRef]
26. Wang, J.; Jin, W.; Cui, Y.-F.; Zhang, W.-F.; Wu, C.-H.; Alessandro, P. Earthquake-triggered landslides affecting a UNESCO Natural Site: The 2017 Jiuzhaigou earthquake in the World national park, China. *J. Mt. Sci.* **2019**, *15*, 1412–1428. [CrossRef]
27. Cui, P.; Liu, S.; Tang, B.; Chen, X. *Research and Prevention of Debris Flow in National Parks*; Science Press: Beijing, China, 2005.
28. Gan, J.J.; Liu, M.S.; Huang, R.Q.; Fan, C.R.; Li, Q.Y.; Wang, C.Y. A study of hydrological cycle in the Jiuzhaigou core scenic area. *Hydrogeol. Eng. Geol.* **2010**, *37*, e39.
29. Yin, G.; Fan, X.; Guo, J.Q. Isotope Tracer on Water Cycly System in Jiuzaigou, Sichuan. *Acta Geogr. Sin.* **2000**, *67*, 487–494. [CrossRef]
30. Deng, G. Study of Tourism Geosciences Landscape Formation and Protection of Jiuzhaigou World Natural Heritage Site. Ph.D. Thesis, Chengdu University of Technology, Chengdu, China, 2011.

31. Fang, L.; Wu, J.; Su, J.; Wang, M.; Jiang, C.; Fan, L.; Wang, W.; Wang, C.; Tan, X. Relocation of mainshock and aftershock sequence of the M_s7.0 Sichuan Jiuzhaigou earthquake. *Chin. Sci. Bull.* **2018**, *63*, 649–662. [CrossRef]
32. Sun, J.B.; Yue, H.; Shen, Z.K.; Fang, L.H.; Zhan, Y.; Sun, X.Y. The 2017 Jiuzhaigou Earthquake: A Complicated Event Occurred in a Young Fault System. *Geophys. Res. Lett.* **2018**, *45*, 2230–2240. [CrossRef]
33. Xie, Z.; Zheng, Y.; Yao, H.; Fang, L.; Zhang, Y.; Liu, C.; Wang, M.; Shan, B.; Zhang, H.; Ren, J. Preliminary analysis on the source properties and seismogenic structure of the 2017 M_s7.0 Jiuzhaigou earthquake. *Sci. China Earth Sci.* **2018**, *61*, 339–352. [CrossRef]
34. Zhao, D.; Qu, C.; Shan, X.; Gong, W.; Zhang, Y.; Zhang, G. InSAR and GPS derived coseismic deformation and fault model of the 2017 M_s7.0 Jiuzhaigou earthquake in the Northeast Bayanhar block. *Tectonophysics* **2018**, *726*, 86–99. [CrossRef]
35. Fan, X.; Scaringi, G.; Xu, Q.; Zhan, W.; Dai, L.; Li, Y.; Pei, X.; Yang, Q.; Huang, R. Coseismic landslides triggered by the 8th August 2017 M_s7.0 Jiuzhaigou earthquake (Sichuan, China): Factors controlling their spatial distribution and implications for the seismogenic blind fault identification. *Landslides* **2018**, *15*, 967–983. [CrossRef]
36. Li, Y.; Huang, C.; Yi, S.; Wu, C. Study on seismic fault and source rupture tectonic dynamic mechanism of Jiuzhaigou M_s7.0 earthquake. *J. Eng. Geol.* **2017**, *25*, 1141–1150.
37. Lugli, S.; Tang, Y.; Reghizzi, M.; Qiao, X.; Schreiber, B.C.; Deng, G. Seasonal Pattern In the High-Elevation Fluvial Travertine From the Jiuzhaigou National Nature Reserve, Sichuan, Southwestern China. *J. Sediment. Res.* **2017**, *87*, 253–271. [CrossRef]
38. Clark, I.; Fritz, P. The environmental isotopes. In *Environmental Isotopes in Hydrogeology*; CRC Press: Boca Raton, FL, USA, 1997; pp. 2–34.
39. Fritz, P.; Cherry, J.; Sklash, M.; Weyer, K. Storm runoff analysis using environmental isotopes and major ions. In *Interpretation of Environmental Isotope and Hydrochemical Data in Groundwater Hydrology*; International Atomic Energy Agency (IAEA): Vienna, Austria, 1976.
40. Mook, W.; Groeneveld, D.; Brouwn, A.; Van Ganswijk, A. Analysis of a run-off hydrograph by means of natural ^{18}O. In *Isotope Techniques in Groundwater Hydrology*; Proceedings of a Symposium; UNESCO: Paris, France, 1974; Volume I.
41. Sklash, M.G.; Farvolden, R.N. The role of groundwater in storm runoff. *J. Hydrol.* **1979**, *43*, 45–65. [CrossRef]
42. Zhou, J.; Wu, J.; Liu, S.; Zeng, G.; Qin, J.; Wang, X.; Zhao, Q. Hydrograph separation in the headwaters of the shule river basin: Combining water chemistry and stable isotopes. *Adv. Meteorol.* **2015**, *2015*, 830306. [CrossRef]
43. Gibson, J.J.; Edwards, T.W.D.; Birks, S.J.; Amour, N.S.; Buhay, W.M.; Mceachern, P.; Wolfe, B.B.; Peters, D.L. Progress in isotope tracer hydrology in Canada. *Hydrol. Process.* **2005**, *19*, 303–327. [CrossRef]
44. Kong, Y.; Pang, Z. Evaluating the sensitivity of glacier rivers to climate change based on hydrograph separation of discharge. *J. Hydrol.* **2012**, *434*, 121–129. [CrossRef]
45. Laudon, H.; Slaymaker, O. Hydrograph separation using stable isotopes, silica and electrical conductivity: An alpine example. *J. Hydrol.* **1997**, *201*, 82–101. [CrossRef]
46. Kong, Y.; Pang, Z. Isotope hydrograph separation in alpine catchments: A review. *J. Glaciol. Geocryol.* **2010**, *3*, 86–91.
47. Genereux, D. Quantifying uncertainty in tracer-based hydrograph separations. *Water Resour. Res.* **1998**, *34*, 915–919. [CrossRef]
48. Klaus, J.; McDonnell, J.J. Hydrograph separation using stable isotopes: Review and evaluation. *J. Hydrol.* **2013**, *505*, 47–64. [CrossRef]
49. Dimova, N.T.; Burnett, W.C. Evaluation of groundwater discharge into small lakes based on the temporal distribution of radon-222. *Limnol. Oceanogr.* **2011**, *56*, 486–494. [CrossRef]
50. Danckwerts, P.V. Significance of liquid-film coefficients in gas absorption. *Ind. Eng. Chem.* **1951**, *43*, 1460–1467. [CrossRef]
51. Zhao, D.; Wang, G.; Liao, F.; Yang, N.; Jiang, W.; Guo, L.; Liu, C.; Shi, Z. Groundwater-surface water interactions derived by hydrochemical and isotopic (222Rn, deuterium, oxygen-18) tracers in the Nomhon area, Qaidam Basin, NW China. *J. Hydrol.* **2018**, *565*, 650–661. [CrossRef]
52. Craig, H. Isotopic variations in meteoric waters. *Science* **1961**, *133*, 1702–1703. [CrossRef]

53. Kong, Y.; Wang, K.; Li, J.; Pang, Z. Stable isotopes of precipitation in China: A consideration of moisture sources. *Water* **2019**, *11*, 1239. [CrossRef]
54. Michel, R.L. Tritium in the hydrologic cycle. In *Isotopes in the Water Cycle: Past, Present and Future of a Developing Science*; Aggarwal, P.K., Gat, J.R., Froehlich, K.F.O., Eds.; Springer: Dordrecht, The Netherlands, 2005; pp. 53–66. [CrossRef]
55. Solomon, D.; Cook, P. *Environmental Tracers in Subsurface Hydrology*; Cook, P.G., Herczeg, A.L., Eds.; Kluwer Academic Publishers: Boston, MA, USA, 2000; pp. 397–424. [CrossRef]
56. Pang, Z.; Kong, Y.; Froehlich, K.; Huang, T.; Yuan, L.; Li, Z.; Wang, F. Processes affecting isotopes in precipitation of an arid region. *Tellus B* **2011**, *63*, 352–359. [CrossRef]
57. Babiker, M.; Gudmundsson, A. The effects of dykes and faults on groundwater flow in an arid land: The Red Sea Hills, Sudan. *J. Hydrol.* **2004**, *297*, 256–273. [CrossRef]
58. Hinton, M.J.; Schiff, S.L.; English, M.C. Examining the contributions of glacial till water to storm runoff using two- and three-component hydrograph separations. *Water Resour. Res.* **1994**, *30*, 983–993. [CrossRef]
59. Wels, C.; Cornett, R.J.; Lazerte, B.D. Hydrograph separation: A comparison of geochemical and isotopic tracers. *J. Hydrol.* **1991**, *122*, 253–274. [CrossRef]
60. Gat, J.R. Stable isotopes of fresh and saline lakes. In *Physics and Chemistry of Lakes*; Lerman, A., Imboden, D.M., Gat, J.R., Eds.; Springer: Berlin/Heidelberg, Germany, 1995; pp. 139–165. [CrossRef]

Publisher's Note: MDPI stays neutral with regard to jurisdictional claims in published maps and institutional affiliations.